



RESEARCH ARTICLE

Melanin nanoparticles enhance the neuroprotection of mesenchymal stem cells against hypoxic-ischemic injury by inhibiting apoptosis and upregulating antioxidant defense

Chunliu Tang^{1,2}  | Jiefeng Luo³ | Xianjia Yan⁴ | Qiaojuan Huang⁵ |
Zhenhua Huang⁶ | Qi Luo¹ | Yuan Lan¹ | Dingzhi Chen¹ | Baolin Zhang⁴ |
Menghua Chen⁷ | Deyan Kong³ 

¹Graduate School, Guangxi Medical University, Nanning, Guangxi, China

²Department of Emergency, The Second Affiliated Hospital of Guangxi Medical University, Nanning, Guangxi, China

³Department of Neurology, The Second Affiliated Hospital of Guangxi Medical University, Nanning, Guangxi, China

⁴Key Laboratory of New Processing Technology for Nonferrous Metal & Materials, Guangxi Key Laboratory of Optical and Electronic Materials and Devices, College of Materials Science and Engineering, Guilin University of Technology, Ministry of Education, Guilin, Guangxi, China

⁵Department of Cardiology, The Second Affiliated Hospital of Guangxi Medical University, Nanning, Guangxi, China

⁶Department of Urology, National Hospital of Guangxi Zhuang Autonomous Region, Nanning, Guangxi, China

⁷Intensive Care Unit, The Second Affiliated Hospital of Guangxi Medical University, Nanning, Guangxi, China

Correspondence

Baolin Zhang, Key Laboratory of New Processing Technology for Nonferrous Metal & Materials, Guangxi Key Laboratory of Optical and Electronic Materials and Devices, College of Materials Science and Engineering, Guilin University of Technology, Ministry of Education, 12# Jian Gan Rd Guilin 541004, Guangxi, China.
Email: zhangbaolin@glut.edu.cn

Menghua Chen, Intensive Care Unit, The Second Affiliated Hospital of Guangxi Medical University, 166# Eastern University Rd, Nanning 530000, Guangxi, China.
Email: cmhnn@sina.com

Deyan Kong, Department of Neurology, The Second Affiliated Hospital of Guangxi Medical University, 166# Eastern University Rd, Nanning 530000, Guangxi, China.
Email: kongdeyaxnn@163.com

Abstract

Polydopamine nanoparticles are artificial melanin nanoparticles (MNPs) that show strong antioxidant activity. The effects of MNPs on the neuroprotection of mesenchymal stem cells (MSCs) against hypoxic-ischemic injury and the underlying mechanism have not yet been revealed. In this study, an oxygen–glucose deprivation (OGD)-injured neuron model was used to mimic neuronal hypoxic-ischemic injury in vitro. MSCs pretreated with MNPs and then cocultured with OGD-injured neurons were used to investigate the potential effects of MNPs on the neuroprotection of MSCs and to elucidate the underlying mechanism. After coculturing with MNPs-pretreated MSCs, MSCs, and MNPs in a transwell coculture system, the OGD-injured neurons were rescued by 91.24%, 79.32%, and 59.97%, respectively. Further data demonstrated that MNPs enhanced the neuroprotection against hypoxic-ischemic injury of MSCs by scavenging reactive oxygen species and superoxide and attenuating neuronal apoptosis by deactivating caspase-3, down-regulating the expression of proapoptotic Bax proteins, and upregulating the expression of antiapoptotic Bcl-2 proteins. These findings suggest that MNPs enhance the neuroprotective effect of MSCs against hypoxic-ischemic injury by inhibiting apoptosis and upregulating antioxidant defense, which could provide some

Chunliu Tang, Jiefeng Luo, and Xianjia Yan contributed equally to this study.

This is an open access article under the terms of the Creative Commons Attribution-NonCommercial-NoDerivs License, which permits use and distribution in any medium, provided the original work is properly cited, the use is non-commercial and no modifications or adaptations are made.

© 2022 The Authors. *Cell Biology International* published by John Wiley & Sons Ltd on behalf of International Federation of Cell Biology.

evidence for the potential application of combined MNPs and MSCs in the therapy for ischemic stroke.

KEYWORDS

antioxidant, apoptosis, ischemic stroke, melanin nanoparticles, mesenchymal stem cells

1 | INTRODUCTION

Ischemic stroke is one of the leading causes of long-term disability and mortality worldwide and is in urgent need of new therapeutic strategies. Current therapeutic interventions for ischemic stroke are limited to intravenous administration of tissue plasminogen activator and endovascular treatment, which aim to recanalize blood flow before major brain damage occurs (Goyal et al., 2015; Muchada et al., 2014). However, these therapies have strict time window requirements, thus only a small number of people can benefit from them. Mesenchymal stem cell (MSC) infusion is a potential treatment for ischemic stroke for patients with no other options. Both bench experiments and clinical trials have shown that MSCs are safe, feasible, and potentially efficacious in the treatment of stroke (Moniche et al., 2012; Prasad et al., 2012; Savitz et al., 2011). MSC transplantation could also promote the improvement of neurological function and reduce infarct volume after cerebral ischemia in a stroke model (Bao et al., 2011; Lee et al., 2016). However, a large number of transplanted MSCs undergo cell death, which affects the therapeutic effect of transplanted MSCs due to the adverse microenvironment induced by hypoxia-ischemia (N. Liu et al., 2011; Zhu et al., 2006). The low survival rate of transplanted MSCs may be related to many factors, such as intense inflammation and oxidative stress (OS), a large number of proapoptotic factors and chemokines, and the lethal effect of ischemia-reperfusion injury on transplanted cells. Therefore, it is urgent to explore innovative methods to promote the survival of transplanted stem cells under hypoxic-ischemic conditions to enhance the efficacy of stem cells in the treatment of ischemic stroke.

With the development of nanomedicine, a wide range of nanoparticles with antioxidation effects have been formulated for the treatment of ischemic stroke. Among these, natural and artificial melanin nanoparticles (MNPs), including polydopamine nanoparticles (PDA NPs), have the potential to be translated to the clinic due to their potent antioxidation and good biocompatibility. PDA NPs remarkably reduced intracellular reactive oxygen species (ROS) levels in murine macrophages challenged with either H₂O₂ or lipopoly-saccharide. In murine models of both acute peritonitis and acute lung injury (ALI), PDA NPs diminished ROS generation, reduced proinflammatory cytokines, attenuated neutrophil infiltration, and alleviated lung tissue damage (Zhao et al., 2018). Ultrasmall Mn²⁺-chelated melanin (MMP) nanoparticles incorporated with polyethylene glycol (MMPP) could scavenge multiple ROS and suppress ROS-induced OS *in vitro* (Sun et al., 2019). Recently, researchers revealed that melanin-like nanoparticles derived from the self-polymerization of 1,8-dihydroxynaphthalene (PDH

nanoparticles) could not only act as radical scavengers to alleviate OS but could also chelate calcium overload to suppress the endoplasmic reticulum stress response and showed a significant anti-inflammation therapeutic effect on ALI mice (Lou et al., 2021). To date, the potential of MNPs in antioxidative therapy for ischemic stroke remains poorly explored. A study demonstrated that MNPs reduced cell death by reducing ROS levels, preventing Bax upregulation and Bcl-2 downregulation in Neuro2A cells treated with CoCl₂ and significantly decreasing the infarct area in an ischemic stroke model (Liu et al., 2017). Since MNPs have potential anti-inflammatory and antioxidant effects, MNPs may enhance the survival of transplanted stem cells in an ischemic and hypoxic environment, thereby enhancing the neuroprotective effects of stem cells. Moreover, MNPs can be directly internalized by MSCs without any noticeable influence on cell viability (Cai et al., 2020). However, whether MNPs internalized by MSCs can enhance the neuroprotective effect of MSCs remains unclear. In this study, we aimed to establish the potential effects of MNPs on the neuroprotection of MSCs and investigate the underlying mechanism.

2 | MATERIALS AND METHODS

2.1 | Synthesis of MNPs

MNPs were synthesized according to the reported method (Ju et al., 2011), with only minor modifications. In brief, an aqueous solution containing dopamine (DA) hydrochloride was prepared by dissolving 119.7 mg of DA hydrochloride (Aladdin Biochemical Technology Co., Ltd.) in 90 ml of deionized water and stirring vigorously. The solution was heated from room temperature to 70°C, and then 760 µl of 1N NaOH (Chemical Co., Ltd.) was added and heated at 70°C for 5 h. After the addition of NaOH, the solution first turned light brown and then gradually turned dark brown. To obtain MNPs, the resulting product was cooled to room temperature at the end of the reaction, washed three times with deionized water, and centrifuged at 16,000 rpm. Then, MNPs were stored in a refrigerator at 4°C for subsequent use.

2.2 | Characterizations of MNPs

The morphology and size of MNPs were observed by scanning electron microscopy (SEM; Hitachi S-4800) at an accelerating voltage of 5 kV. The hydrated particle size and zeta potential of the MNPs

were determined by a Malvern Zetasizer particle analyzer (ZEN3600; Malvern). Fourier transform infrared (FTIR) spectra were recorded on a Fourier infrared spectrometer (Nexus 470 Thermo Nicolet). The ultraviolet-visible (UV-vis) absorption of DA and MNPs was obtained from an UV spectrophotometer (UV 3600; Shimadzu Corporation).

2.3 | Animals

SD rats were purchased from the Experimental Animal Center of Guangxi Medical University. The experimental protocols were performed according to the Guidelines of the Care and Use of Laboratory Animals of the National Institutes of Health and approved by the Ethics and Animal Subject Committee of Guangxi Medical University.

2.4 | Culture and identification of MSCs

Bone marrow MSCs were isolated as described previously with some modification (Kong et al., 2017). Briefly, bone marrow was harvested by flushing isolated from the tibia and femur of newborn Sprague-Dawley rats. The obtained cell suspension was centrifuged, and then the mononuclear cells were suspended in minimum essential medium- α (Gibco, Invitrogen) with 15% fetal bovine serum (Gibco), counted at 1×10^6 /ml and placed in a culture flask. The cells were cultured in a 5% CO₂ incubator at 37°C, and the medium was refreshed every 2 days. The primary cultures were subcultured 1:2 when they reached 80%–90% confluence. MSCs were acquired for the following experiments at passages 3–5. The surface antigens of the fourth passage MSCs were identified by flow cytometry. The MSCs were detached with 0.25% trypsin (1.5 ml) containing ethylene diamine tetraacetic acid, centrifuged, resuspended with appropriate phosphate-buffered saline (PBS), and centrifuged at 1200 rpm. The MSCs were then resuspended in 100 μ l PBS to make a single-cell suspension. PE-conjugated CD90 and APC-conjugated CD29 antibodies (5 μ l each; Miltenyi Biotec), fluorescein isothiocyanate-conjugated CD44 (2 μ l; Miltenyi Biotec), PE/cyanine7-conjugated CD45 (5 μ l; Biolegend) or the corresponding isotype control were incubated with the cell suspension for 20 min at room temperature in the dark. Then, the stained cells were resuspended and detected by a flow cytometer (CytoFLEX S; Beckman Coulter).

2.5 | Assay for antioxidant activity of MNPs

The free radical-scavenging capacity of MNPs was detected by the 2,2-diphenyl-1-picrylhydrazyl (DPPH) scavenging method (Brand-Williams et al., 1995). The experiment was carried out according to the instructions of the DPPH free radical scavenging capacity test kit (Solarbio). Briefly, the test was carried out in a 96-well plate using a total volume of 190 μ l working fluid containing DPPH and ethanol and a series of samples with 10 μ l MNP concentrations of 5–200 μ g/ml. A working fluid of 190 μ l with 10 μ l distilled water was

used as a blank control. A total of 190 μ l ethanol containing a series of samples with 10 μ l MNP concentrations of 5–200 μ g/ml was used as a control. The scavenging activity was evaluated by monitoring the absorbance decrease at 515 nm after it remained in the dark for 30 min. Absorbance was measured at 515 nm using the enzyme Labeler (HBS-1096C; DeTie). The measurements were performed in triplicate. DPPH radical scavenging activity was calculated as $(A_{515_{\text{black}}} + A_{515_{\text{control}}} - A_{515_{\text{sample}}})/A_{515_{\text{black}}} \times 100\%$, where $A_{515_{\text{black}}}$ is the absorbance of DPPH solution without MNPs samples, $A_{515_{\text{sample}}}$ is the absorbance of the samples of MNPs mixed with DPPH solution, and $A_{515_{\text{control}}}$ is the absorbance of the samples of MNPs themselves without DPPH solution. The measurements were performed in triplicate.

2.6 | Cytotoxicity assay for MNPs

MSCs were cultured in 96-well plates at a concentration of 10^4 cells/well, and 10 different concentrations of MNPs (ranging from 0 to 200 μ g/ml) were added for 24 h or incubated with MNPs (10, 20, 40, 60, and 80 μ g/ml) for 24, 48, and 72 h. Then, a Cell Counting Kit-8 (CCK-8) assay kit (Sigma-Aldrich) was used to measure the cell viability of MSCs. Normal culture media were used for the control group. Then, 10 μ l CCK-8 solution was added to each well for 1 h at 37°C. Absorbance was measured at 450 nm using the enzyme labeler (HBS-1096C; DeTie). Solutions containing alpha minimum essential medium and CCK-8 without cells were used as blanks. Cell viability (%) = $(A_{450_{\text{sample}}} - A_{450_{\text{blank}}})/(A_{450_{\text{control}}} - A_{450_{\text{blank}}}) \times 100\%$. The best concentration of MNPs (20 μ g/ml) and the best incubation time (24 h) were selected for further experiments. The test was repeated three times.

2.7 | Transmission electron microscopy

Transmission electron microscopy (TEM) was used to observe the uptake and distribution of MNPs in MSCs. MSCs without MNP treatment were used as the untreated control. After incubation with MNPs (20, 40, and 60 μ g/ml) or without MNPs for 24 h, the cells were washed twice with PBS, fixed for 24 h with 2.5% (vol/vol) glutaraldehyde and postfixed for 2 h with 1% (vol/vol) osmium tetroxide. The cells were dehydrated in a graded series of ethanol (30, 50, 75, 90, 99, and 100 vol%). The samples were then embedded in resin after washing with PBS. Sections with a thickness of approximately 60 nm were cut and stained with 2% aqueous uranyl acetate for 1 h in the dark. The pictures were captured with a TEM (Hitachi H-7650).

2.8 | Establishment of in vitro ischemic models of cortical neuron and MSC-neuron coculture systems

The coculture system was established in Transwell® 6-well or 12-well plates with 0.4 μ m polycarbonate membranes (Corning Life Sciences).

The primary neurons were isolated and cultured as described previously (Kong et al., 2017) and identified as at least 95% MAP2-positive cells with immunofluorescence. Primary cortical neurons were cultured in the lower chamber of transwell plates at a density of 2×10^6 cells per well (six-well plates) or 1×10^6 cells per well (12-well plates). Oxygen-glucose deprivation (OGD) was carried out in cultures after 7 days. The primary cortical neurons were washed with deoxygenated, glucose-free PBS buffer, and then the cultures were transferred to an anaerobic incubator containing 5% CO₂ and 95% N₂ at 37°C for 120 min. The non-OGD control neurons were cultured with PBS containing glucose and incubated in normal culture conditions for 120 min. Immediately after OGD, both OGD and non-OGD control neurons were washed with PBS, replaced with fresh neurobasal/B-27 medium, and then placed in normal culture conditions (37°C, 5% CO₂). Immediately after OGD, the upper insert chambers seeded with 5×10^6 MSCs or the same concentration of MSCs pretreated with 20 µg/ml MNPs (MNPs-MSCs) were placed in the transwell system above the lower chamber neurons and then cocultured for 48 h. Neurobasal/B-27 containing 20 µg/ml MNPs was placed in the upper insert chambers of OGD-injured neurons as the treatment control group. Cortical neurons cocultured with plain neurobasal/B-27 medium in the upper insert chambers without ischemic modeling or MSC coculturing served as a negative control.

2.9 | Assessment of neuronal cell death

Neuronal cell death was quantified by a propidium iodide (PI; Invitrogen) uptake assay. A PI/Hoechst staining assay was performed after each experimental treatment for 48 h. The neurons were costained with PI (2.5 µg/ml; Invitrogen) and Hoechst 33342 (1.5 µg/ml; Invitrogen) for 5 min and observed by fluorescence microscopy as described previously (Kong et al., 2017). PI-positive cells (red) were counted as dead cells, and Hoechst 33342-positive cells (blue) were counted as live cells. The percentage of cell death was determined as the ratio of PI-positive cells to Hoechst 33342-positive cells. All experiments were repeated six times, and the average was calculated.

2.10 | Intracellular ROS/superoxide radical assay

Total levels of ROS and superoxide were detected by using the intracellular ROS/superoxide detection assay kit (ab139476; Abcam). Neurons cultivated in coverslips at a density of 1×10^6 cells per well (12-well plates) after the corresponding treatment for 24 h were washed with fresh medium and loaded with the OS detection reagent (1:500) and superoxide detection reagent (1:500) for 30 min at 37°C. For the negative control, an ROS inhibitor (*N*-acetyl-L-cysteine) at a final concentration of 10 mM was added to the cells of the OGD group for 30 min before the detection reagent was loaded. After the cells were washed three times with wash buffer, ROS- and superoxide-positive cells were observed by fluorescence microscopy (OLYMPUS BX53) with the recommended filter set for ROS

detection compatible with fluorescein (Ex/Em = 490/525 nm) and superoxide detection filter set compatible with rhodamine (Ex/Em = 550/620 nm). Increased levels of OS result in uniform green cytoplasmic staining in the presence of the OS detection reagent (green) and a bright orange nuclear staining pattern in the presence of the superoxide detection reagent (red). The mean fluorescence intensity was analyzed with ImageJ software (Media Cybernetics, Inc.). All samples were repeated six times.

2.11 | Immunofluorescence staining

After the corresponding treatment, neurons grown on coverslips (1×10^6 cells per well) were fixed with 4% paraformaldehyde for 30 min, washed with PBS, and then permeabilized with 0.1% Triton X-100 (Sigma-Aldrich). After blocking with 5% bovine serum albumin, the coverslips were incubated at 4°C overnight with anti-rabbit cleaved caspase-3 antibody (1:150; Cell Signaling Technology). The coverslips were then rinsed and incubated with Alexa Fluor 594-conjugated donkey anti-rabbit IgG (1:200; Cell Signaling Technology) for 2 h. After thorough rinsing, the nuclei were stained with 4',6-diamidino-2-phenylindole dihydrochloride (DAPI; 1 µ/ml) and then observed by fluorescence microscopy (OLYMPUS BX53). The number of immunoreactive cells was quantified with ImageJ software (Media Cybernetics, Inc.). Negative controls were performed by omitting the application of the primary antibody. Five different fields for each sample were counted. We calculated the percentage of positive cells with cleaved caspase-3 expression (red) with respect to the total number of DAPI (blue). All counts were conducted by a blinded investigator. Each experiment was replicated six times.

2.12 | Western blot analysis

Total protein samples were extracted from neurons (2×10^6 cells per well, six-well plates) with the corresponding treatment using cell lysis buffer for western blot analysis (Solarbio). The concentration of the proteins was measured using a bicinchoninic acid assay. After boiling for 10 min, the samples were separated by sodium dodecyl sulfate-polyacrylamide gel electrophoresis (12% polyacrylamide gels), transferred to polyvinylidene fluoride membranes (Solarbio), and blocked with 5% nonfat milk for 2 h at room temperature. The polyvinylidene fluoride membranes were then incubated with the following primary antibodies: Bcl-2 (1:1000; Abcam), cleaved caspase-3, Bax, and β-actin (1:1000; all purchased from Cell Signaling Technology) at 4°C for 12 h. The membranes were washed three times with Tris-buffered saline containing Tween 20 (TBST; Solarbio) and then incubated with a secondary antibody anti-rabbit immunoglobulin G (IgG) (H+L) (1:2000; Cell Signaling Technology) for 1 h at room temperature. After washing with TBST three times, the signals were visualized using a chemiluminescent imaging system (GelView6000M; BLT). The relative expression of each target protein was determined by Quantity One software 4.6.2 (Bio-Rad) and normalized to that of

β -actin. Experiments were repeated six times, and the average was calculated.

2.13 | Statistical analysis

Data are presented as the mean \pm SEM. One-way analysis of variance was applied for multiple comparisons followed by Tukey's post-hoc test. Statistical analysis was conducted using SPSS software version 23.0 (SPSS Inc.). Statistical significance was defined as $p < .05$.

3 | RESULTS

3.1 | Characterizations of MNPs

The dimensions of the MNPs were characterized by SEM (Hitachi S-4800) at an accelerating voltage of 5 kV. A small amount of dried powder was dipped on the conductive adhesive, and then the unstuck powder was blown off by using an airbag. After being sprayed with gold, the sample was fixed on the sample holder for SEM observation. As shown by SEM in Figure 1a, the MNPs were uniform nanospheres, with an average diameter of 115.13 ± 8.02 nm.

The size of hydrated particles is the size of nanoparticles in the solution state, also known as the hydrodynamic diameter, including

the core of the nanoparticle and the micelle and adsorbed water on the surface. After the nanoparticles were diluted to an appropriate concentration, ultrasonic dispersion was conducted for approximately 1 min, and then the hydration particle size was measured directly. The pH of the diluted sample was adjusted to 7 and then tested for zeta potential. As shown in Figure 1b, the average hydrated particle size of MNPs is 106.5 nm (polymer dispersity index: 0.340 ± 0.010). Zeta potential analysis revealed that the surface of the MNPs was negatively charged (-21.3 mV; Figure 1c).

The FTIR spectra of DA and MNPs are shown in Figure 1d, confirming the successful polymerization of DA. The broad peak in the range of $3700\text{--}2800\text{ cm}^{-1}$ was attributed to the tensile vibration of indole and phenol, while the peak at 1621 cm^{-1} was assigned to the stretching vibration of aromatic rings and bending vibration of N-H. The peak at 1141 cm^{-1} can be attributed to the C-O vibration (Fu et al., 2015). The peak at 1401 cm^{-1} corresponds to the bending vibration of phenolic C-O-H (Fu et al., 2016; Tarangini & Mishra, 2014). These results indicate that DA had been successfully polymerized.

The UV-vis absorption of DA and MNPs is represented in Figure 1e, and the obtained broad-band absorption spectra and the primary absorption are in the UV range. Compared with DA monomers, the synthesized MNPs exhibited a wide range of absorption from UV to near-infrared (NIR) wavelengths. The reason for the absorption phenomenon in the UV region of the spectrum

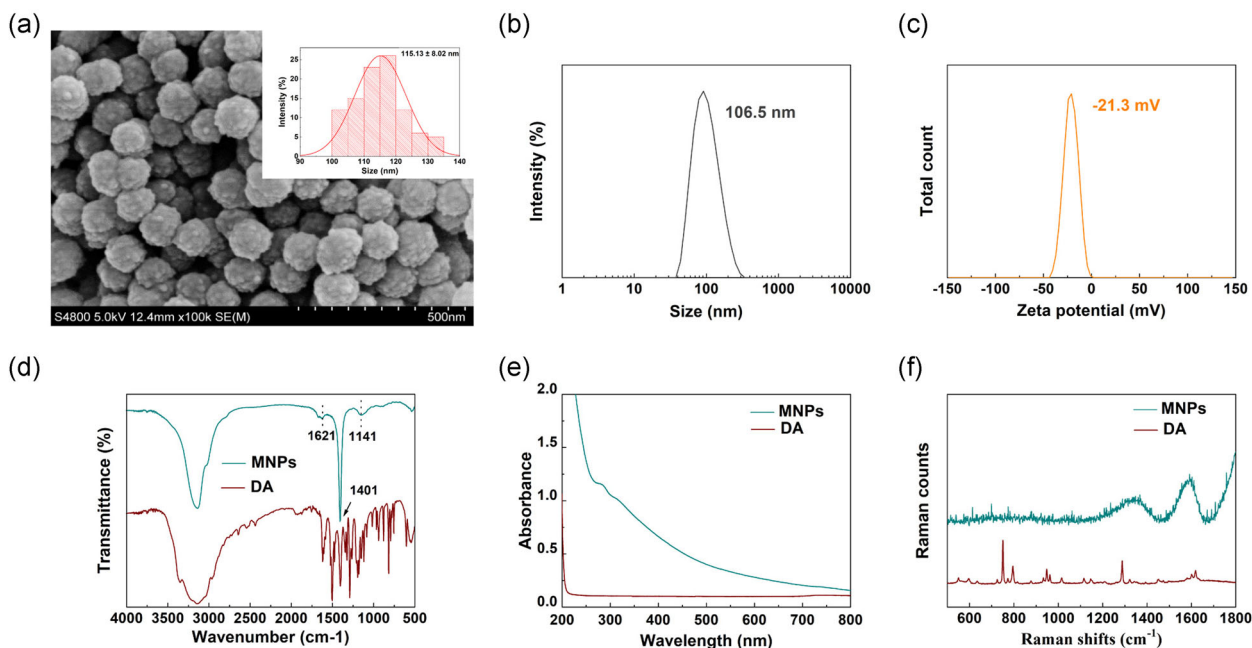


FIGURE 1 Characterization of MNPs. (a) SEM images and size distributions of MNPs. The MNPs were uniform nanospheres, with an average diameter of 115.13 ± 8.02 nm. (b) The hydrodynamic diameter of MNPs was 106.5 nm. (c) Zeta potential of MNPs was -21.3 mV. (d) FTIR spectra of DA and MNPs. There was a broad peak in the range of $3700\text{--}2800\text{ cm}^{-1}$, and the peaks at 1621, 1401, and 1141 cm^{-1} . (e) UV-vis absorption spectra of DA and MNPs. The obtained broad-band absorption spectra and the primary absorption are in the UV range. Compared with DA monomers, the synthesized MNPs exhibited a wide range of absorption from UV to NIR wavelengths. (f) Raman spectra of DA and MNP. There were characteristic peaks of MNPs at 1594 and 1360 cm^{-1} . DA, dopamine; FTIR, Fourier transform infrared spectroscopy; MNP, melanin nanoparticle; NIR, near-infrared; SEM, scanning electron microscopy; UV-vis, ultraviolet-visible

is that DA was oxidized into dopachrome and dopaindole, and the subsequent self-polymerization process led to an obvious absorption from visible light to NIR wavelengths (Liu et al., 2013). The Raman spectra of DA and MNPs are presented in Figure 1f. Characteristic peaks at 1594 and 1360 cm^{-1} can be attributed to the stretching and deformation of the aromatic ring on MNPs (Li et al., 2013).

3.2 | Effect of MNPs on MSC viability and cellular localization of uptaken nanoparticles

The following surface markers of BMSCs were identified using flow cytometry at the fourth generation: positive markers, CD29 (99.8%),

CD44 (98.5%), and CD90 (97.7%); and negative markers, CD45 (2.4%) (Figure 2a–d).

Under our experimental conditions, the free radical scavenging rate of MNPs increased from 2.04% to 38.58% as the concentration of MNPs increased (Figure 3a). The free radical scavenging activity of MNPs increased in a dose-dependent manner.

The influence of MNPs on the viability of MSCs was evaluated by a CCK-8 assay. First, cell viability was tested with ten different concentrations of MNPs. In detail, 24 h after MSC seeding, MNPs at concentrations ranging from 5 to 200 $\mu\text{g}/\text{ml}$ were added to the culture medium and incubated with MSCs for 24 h. The results showed that MNPs at concentrations of 20 and 40 $\mu\text{g}/\text{ml}$ displayed significantly higher cell viability than the control group (MSCs grown without MNPs in culture; $n = 3$,

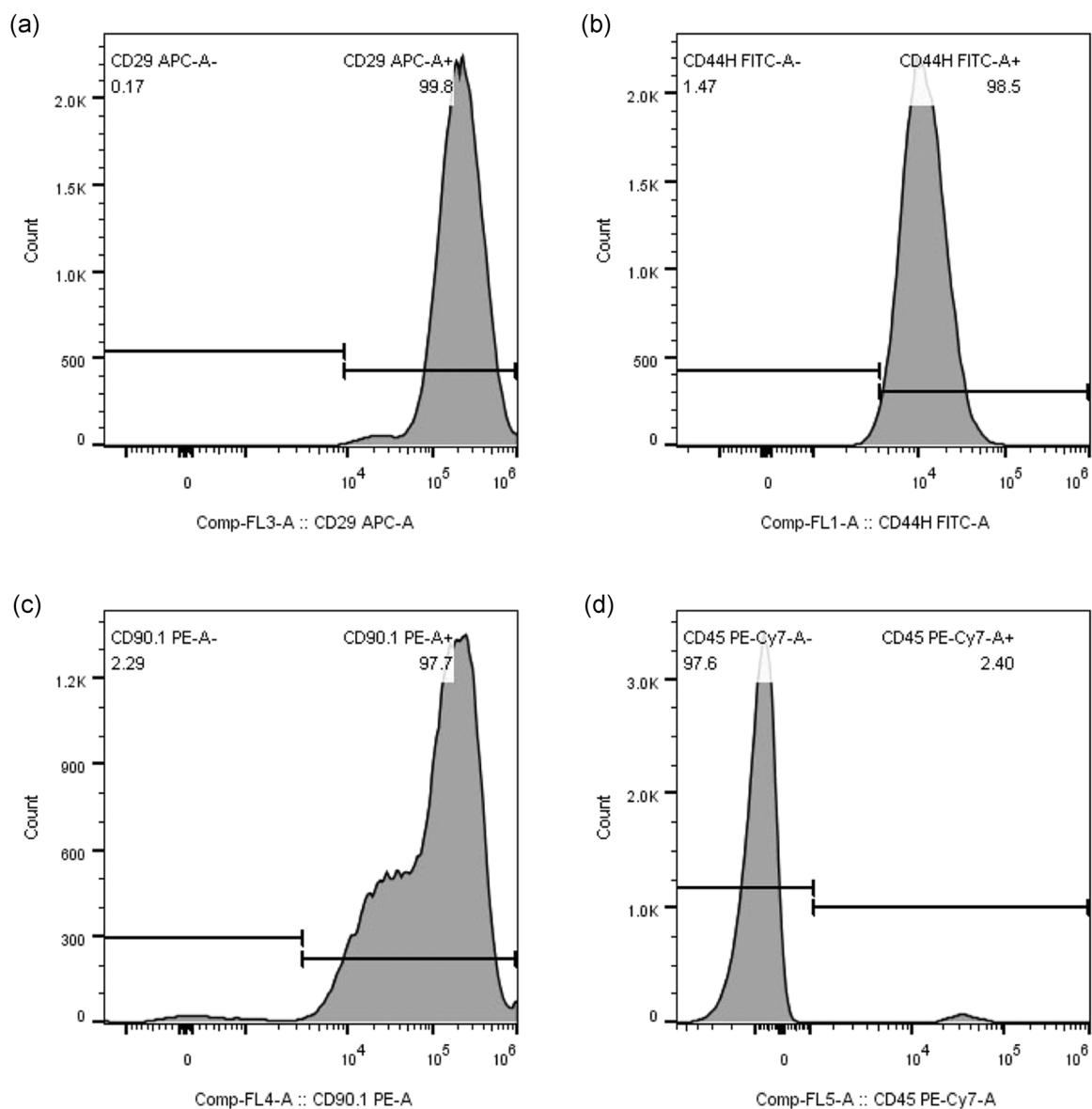


FIGURE 2 Identification of the MSCs. The surface markers of the MSCs were analyzed by flow cytometry (a–d). The results of CD phenotypic antigen identification were CD29+ (a), CD44+ (b), CD90+ (c), and CD45– (d). MSC, mesenchymal stem cell

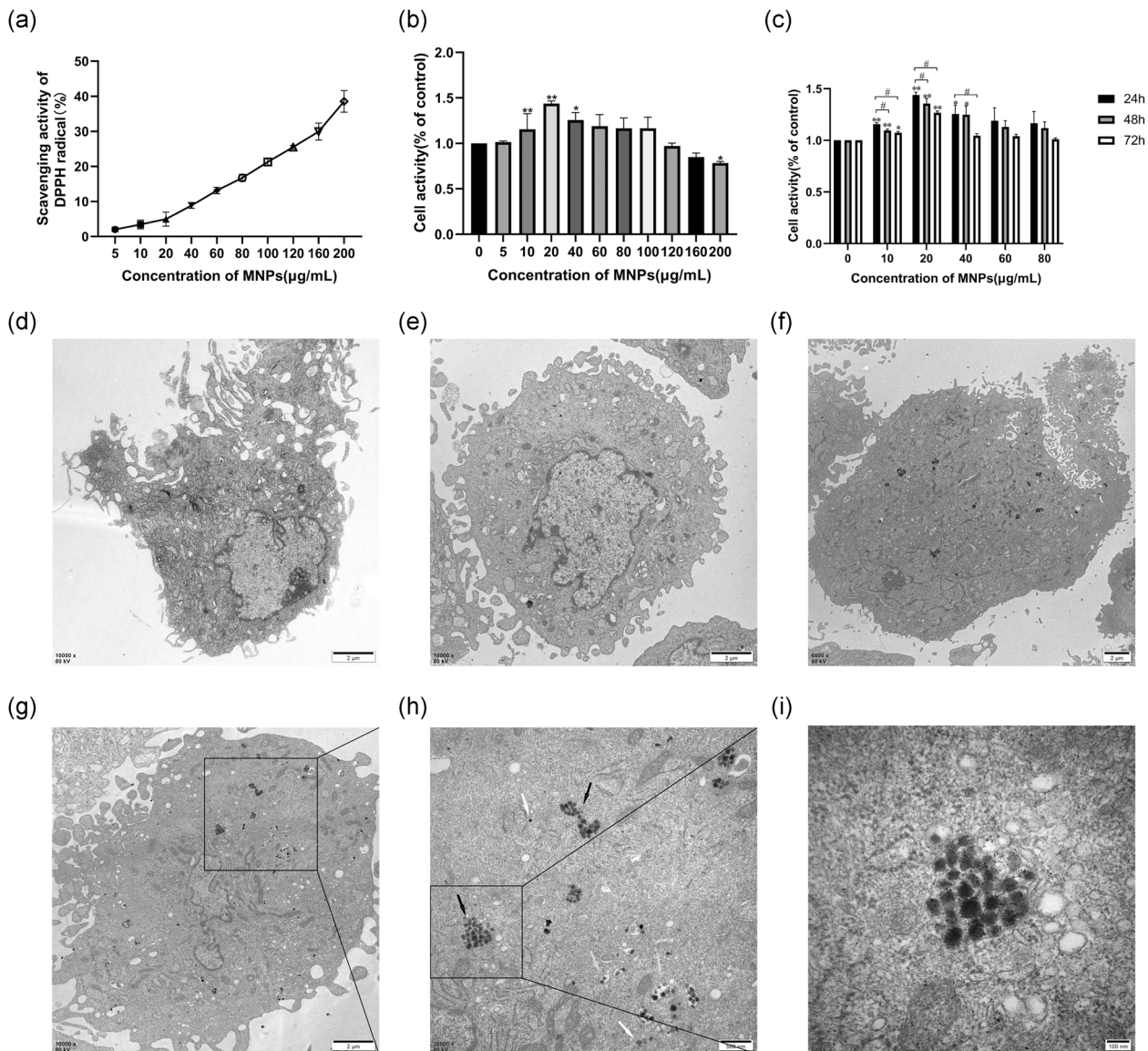


FIGURE 3 Antioxidant activity of MNPs, cell viability, and TEM images of ultrathin sections of MSCs. (a) DPPH radical scavenging activity of MNPs. Various concentrations of 10 μ l MNPs (5–200 μ g/ml) and 190 μ l working fluid containing DPPH and ethanol were placed in a 96-well plate. A working fluid of 190 μ l with 10 μ l distilled water was used as a blank control. A total of 190 μ l ethanol containing a series of samples with 10 μ l MNPs concentrations of 5–200 μ g/ml was used as a control. The scavenging activity was evaluated by monitoring the absorbance decrease at 515 nm after it remained in the dark for 30 min. The free radical scavenging activity of MNPs increased in a dose-dependent manner. (b–c) MSCs were seeded in 96-well plates at a density of 1×10^4 cells per well for 24 h and then treated with different concentrations of MNPs for 24, 48, or 72 h. Cell viability was tested by CCK-8 assay. (b) Viability of MSCs incubated with increasing concentrations of MNPs (ranging from 0 to 200 μ g/ml) for 24 h. MNPs at concentrations of 20 and 40 μ g/ml displayed significantly higher cell viability than the control group, and a significant decrease in cell viability was first observed at a concentration of 200 μ g/ml. (c) MSCs were treated with various concentrations of MNPs (10, 20, 40, 60, and 80 μ g/ml) for 24, 48, and 72 h. MSCs that were not incubated with MNPs served as the control group. After 48 and 72 h, the cell viability started decreasing significantly for the concentrations of 10 and 20 μ g/ml, with a far lower viability than after 24 h. (c–h) TEM images of ultrathin sections of MSCs, (d) Untreated control, (e) MSCs were treated with 20 μ g/ml MNPs for 24 h, (f) MSCs were treated with 40 μ g/ml MNPs for 24 h, (g) MSCs were treated with 60 μ g/ml MNPs for 24 h, (h) Magnification of the selected area in (g), (i) magnification of the selected area in (h). Clusters (black arrow) or free (white arrow) MNPs in the cytoplasm were observed. In addition, autophagic vacuoles (AVs) with MNPs were also observed (yellow arrow). All data are described as the mean \pm SEM, * p < .05, ** p < .01 compared with the control group, # p < .05 compared with the 24 h group. Scale bar = 2 μ m (d–g), 500 nm (h), 100 nm (i). CCK-8, Cell Counting Kit-8; DPPH, 2,2-diphenyl-1-picrylhydrazyl; MNP, melanin nanoparticle; MSC, mesenchymal stem cell; TEM, transmission electron microscopy

$p < .05$; Figure 3b). A significant decrease in cell viability was first observed at a concentration of 200 $\mu\text{g/ml}$ ($n = 3$, $p < .05$; Figure 3b). Cells were incubated with MNPs at five different concentrations (10, 20, 40, 60, 80 $\mu\text{g/ml}$) for 24, 48, and 72 h, respectively. Figure 3c depicts the time-dependent toxicity of MNPs in MSCs. After 48 and 72 h, the cell viability started decreasing significantly for the concentrations of 10 and 20 $\mu\text{g/ml}$, with a far lower viability than after 24 h ($n = 3$, $p < .05$; Figure 3c). Thus, MNPs at 20 $\mu\text{g/ml}$ incubated with MSCs for 24 h were chosen for further investigation.

TEM was used to detect the uptake and distribution of MNPs in MSCs treated with MNPs (20, 40, and 60 $\mu\text{g/ml}$) for 24 h. Figure 3e–i shows that MNPs were internalized by phagocytosis and endocytic vacuole formation. Figure 3e–g shows that there was an increasing amount of uptaken particles with increasing concentrations of MNPs. The particles were either dispersed in the cytoplasm or distributed in vesicles,

probably lysosomes or late endosomes, and they were either single or aggregated in the MSCs (Figure 3h). There were no negative changes in the cellular ultrastructure of MSCs treated with MNPs (Figure 3e–h).

3.3 | MNPs enhance the protection of MSCs against OGD-injured neurons

To verify whether MNPs enhance the protection of MSCs against OGD-injured neurons, PI/Hoechst double staining was performed. After 120 min of OGD exposure, immediate coculture with MNPs–MSCs (MSCs pretreated with MNPs) for 48 h significantly reduced neuronal cell death (Figure 4a,b, $7.04 \pm 0.533\%$ vs. $80.41 \pm 2.831\%$; $p < .01$, $n = 6$). Treatment with MSCs or MNPs also decreased neuronal cell death by 79.32% ($16.63 \pm 0.811\%$ vs. $80.41 \pm 2.831\%$; $p < .01$, $n = 6$) and 59.97% ($32.19 \pm 1.209\%$ vs.

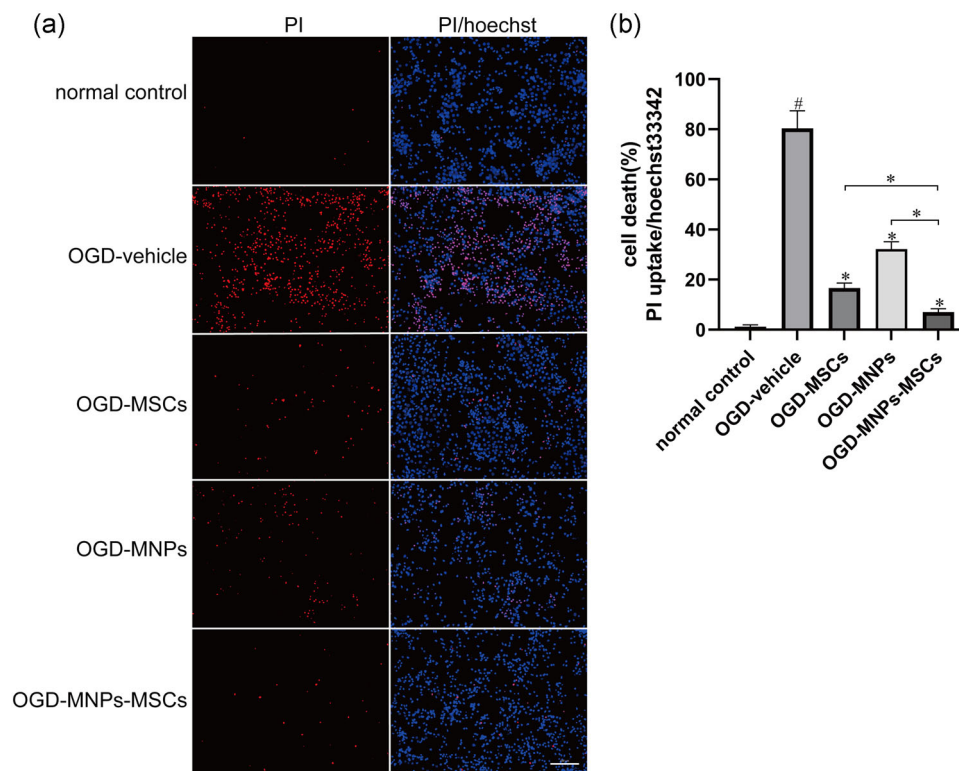


FIGURE 4 MNPs–MSCs reduced OGD-induced neuronal death, and neuroprotection was superior to that of MSCs or MNPs. Primary cortical neurons were cultured on coverslips in 12-well culture plates at a density of 1×10^6 cells per well for 7 days. Immediately after OGD, the upper insert chambers seeded with 5×10^6 MSCs (OGD–MSCs group) or the same concentration of MSCs pretreated with 20 $\mu\text{g/ml}$ MNPs (OGD–MNPs–MSCs group) were placed in the transwell system above the lower chamber neurons and then cocultured for 48 h. Neurobasal/B-27 containing 20 $\mu\text{g/ml}$ MNPs was placed in the upper insert chambers of OGD-injured neurons for 48 h as the OGD–MNPs group. Cortical neurons cocultured with plain neurobasal/B-27 medium in the upper insert chambers without ischemic modeling or MSCs coculturing served as a negative control. A PI/Hoechst staining assay was performed after each experimental treatment. Ratio of PI-positive (labeled dead cells red) cells to Hoechst 33342-positive (labeled all cells blue) cells as the percentage of cell death. (a, b) OGD injury resulted in dramatic cell death as presented by nuclear PI staining, while treatment with MNPs–MSCs or MSCs attenuated neuronal death relative to the OGD vehicle control. Moreover, the neuroprotection of MNPs–MSCs was superior to that of MSCs or MNPs. Scale bar = 100 μm . All data are described as the mean \pm SEM, $\#p < .01$ compared with the normal control; $*p < .01$ compared with the OGD-vehicle group or OGD–MNPs–MSCs group. MNP, melanin nanoparticle; MSC, mesenchymal stem cell; OGD, oxygen–glucose deprivation; PI, propidium iodide

$80.41 \pm 2.831\%$; $p < .01$, $n = 6$), respectively (Figure 4a,b). Treatment with MNPs-MSCs reduced cell death by 91.24%, which was superior to the effect of the OGD-MSCs or OGD-MNPs groups (Figure 4a,b, $7.04 \pm 0.533\%$ vs. $16.63 \pm 0.811\%$, $p < .01$, $n = 6$; $7.04 \pm 0.533\%$ vs. $32.19 \pm 1.209\%$, $p < .01$, $n = 6$).

3.4 | MNPs-MSCs suppressed OGD-induced free radicals in neurons

To determine the antioxidative effect of MNPs-MSCs, an ROS/superoxide detection assay was used to detect the intracellular ROS and

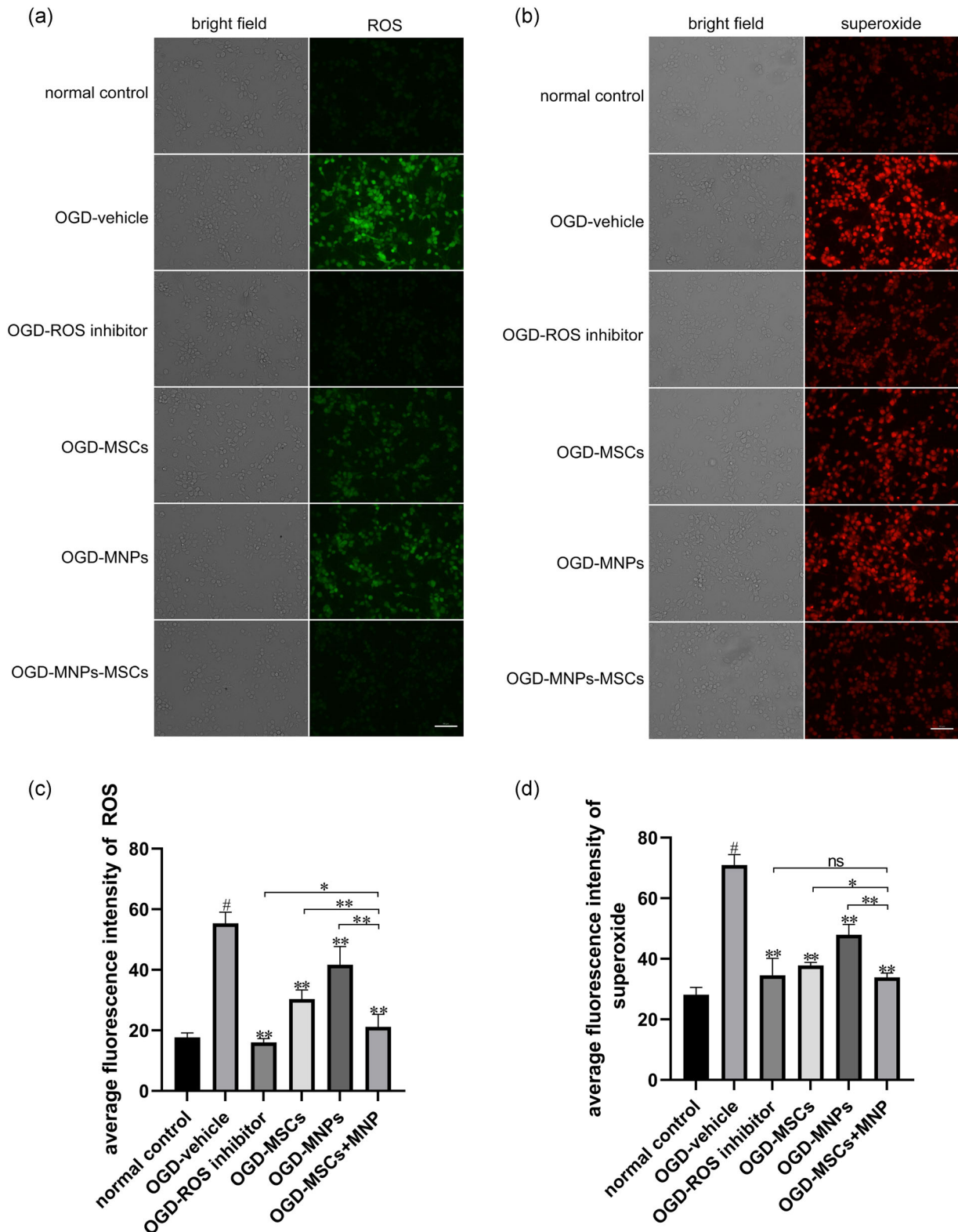


FIGURE 5 (See caption on next page)

superoxide generation in neurons after OGD exposure and the corresponding treatment. As shown in Figure 5a,c, intracellular ROS levels were significantly increased in the OGD-vehicle group compared with the normal control group (55.37 ± 1.49 vs. 17.72 ± 0.60 ; $p < .01$, $n = 6$), while compared with the OGD-vehicle group, treatment with MNPs-MSCs, MSCs, or MNPs decreased OGD-induced ROS production in neurons by 61.80% (21.15 ± 1.71 vs. 55.37 ± 1.49 ; $p < .01$, $n = 6$), 45.13% (30.38 ± 1.23 vs. 55.37 ± 1.49 ; $p < .01$, $n = 6$), and 24.72% (41.68 ± 2.47 vs. 55.37 ± 1.49 ; $p < .01$, $n = 6$), respectively. Meanwhile, treatment with MNPs-MSCs, MSCs, or MNPs also reduced the superoxide levels in OGD-damaged neurons by 52.26% (33.87 ± 1.44 vs. 70.94 ± 1.44 ; $p < .01$, $n = 6$), 46.63% (37.86 ± 0.41 vs. 70.94 ± 1.44 ; $p < .01$, $n = 6$) and 32.37% (47.98 ± 1.38 vs. 70.94 ± 1.44 ; $p < .01$, $n = 6$), respectively (Figure 5b,d; $p < .01$, $n = 6$). Moreover, treatment with MNPs-MSCs remarkably reduced ROS and superoxide production, which was superior to the effect of MSCs or MNPs (Figure 5a,d; $p < .05$, $n = 6$), while treatment with MNPs-MSCs decreased superoxide generation compared to the effect of ROS inhibitors (33.87 ± 1.44 vs. 34.54 ± 2.29 , $p > .05$, $n = 6$; Figure 5d).

3.5 | MNPs enhanced the inhibitory effect of MSCs on neuronal apoptosis after OGD injury

We performed immunofluorescence staining and western blot analysis to determine whether pretreatment with MNPs enhances the protective effect of MSCs against OGD-induced apoptotic cell death. Immunofluorescence staining showed that OGD injury significantly induced the cleavage of caspase-3 in neurons compared with the normal control group (Figure 6a,b; $13.17 \pm 0.897\%$ vs. $0.86 \pm 0.061\%$, $p < .01$, $n = 6$), while treatment with MNPs-MSCs, MSCs, or MNPs significantly reduced cleaved caspase-3 expression by 84.66%, 71.53%, and 56.49% (Figure 6a,b; $2.02 \pm 0.117\%$ vs. $13.17 \pm 0.897\%$, $p < .01$, $n = 6$; $3.75 \pm 0.153\%$ vs. $13.17 \pm 0.897\%$, $p < .01$, $n = 6$; $5.73 \pm 0.269\%$ vs. $13.17 \pm 0.897\%$, $p < .01$, $n = 6$) relative to the OGD vehicle groups. Moreover, the cleaved caspase-3 expression in the OGD-MNPs-MSCs group was significantly lower than that in the OGD-MSCs group or OGD-MNPs group ($2.02 \pm 0.117\%$ vs. $3.75 \pm 0.153\%$, $p < .01$, $n = 6$;

$2.02 \pm 0.117\%$ vs. $5.73 \pm 0.269\%$, $p < .01$, $n = 6$; Figure 6a,b). Furthermore, these results were confirmed by western blot analysis (Figure 6c,d). Western blot analysis showed that the levels of cleaved caspase-3 protein were significantly decreased with the treatment of MNPs-MSCs, MSCs, or MNPs relative to the OGD vehicle group (0.317 ± 0.015 vs. 0.782 ± 0.019 , $p < .01$, $n = 6$; 0.508 ± 0.021 vs. 0.782 ± 0.019 , $p < .01$, $n = 6$; 0.603 ± 0.016 vs. 0.782 ± 0.019 , $p < .01$, $n = 6$; Figure 6c,d). Moreover, the levels of cleaved caspase-3 protein in the OGD-MNPs-MSCs group were significantly lower than those in the OGD-MSCs group or OGD-MNPs group (0.317 ± 0.015 vs. 0.508 ± 0.021 , $p < .01$, $n = 6$; 0.317 ± 0.015 vs. 0.603 ± 0.016 , $p < .01$, $n = 6$; Figure 6c,d). Furthermore, our results demonstrated that the upregulation of proapoptotic Bax and downregulation of antiapoptotic Bcl-2 were involved in OGD-induced cell death in neurons (Bax, 1.372 ± 0.031 vs. 0.805 ± 0.029 , $p < .01$, $n = 6$; Figure 6c,f; Bcl-2, 0.592 ± 0.033 vs. 0.812 ± 0.029 , $p < .01$, $n = 6$; Figure 6c,e), while the treatment with MNPs-MSCs, MSCs, or MNPs prevented Bax upregulation and Bcl-2 downregulation as relative to the OGD vehicle (Bax, 0.943 ± 0.042 vs. 1.372 ± 0.031 , $p < .01$, $n = 6$; 1.065 ± 0.043 vs. 1.372 ± 0.031 , $p < .01$, $n = 6$; 1.168 ± 0.036 vs. 1.372 ± 0.031 ; $p < .01$, $n = 6$; Figure 6c,f; Bcl-2, 1.023 ± 0.051 vs. 0.592 ± 0.033 , $p < .01$, $n = 6$; 0.893 ± 0.032 vs. 0.592 ± 0.033 , $p < .01$, $n = 6$; 0.808 ± 0.049 vs. 0.592 ± 0.033 , $p < .01$, $n = 6$; Figure 6c,e). Moreover, the Bcl-2/Bax ratio in the OGD-MNPs-MSCs group was significantly higher than that in the OGD-MSCs group or OGD-MNPs group (1.093 ± 0.065 vs. 0.849 ± 0.055 , $p < .01$, $n = 6$; 1.093 ± 0.065 vs. 0.697 ± 0.054 , $p < .01$, $n = 6$; Figure 6g). These data demonstrated that the protective effect of MNPs-MSCs against OGD-induced neuronal apoptosis was superior to the effect of MSCs or MNPs.

4 | DISCUSSION

In this study, we found that MNPs enhance the neuroprotective effect of MSCs against hypoxic-ischemic injury by inhibiting apoptosis and upregulating antioxidant defense.

In this study, the observed size and shape of the prepared MNPs (Figures 1a and 3i) were very similar to those reported (Ju et al., 2011;

FIGURE 5 Treatment with MNPs-MSCs significantly attenuated ROS and superoxide production in neurons after OGD toxicity. Primary cortical neurons were cultured on coverslips in 12-well culture plates at a density of 1×10^6 cells per well for 7 days, and the groups were treated as described previously. Neurons cultivated in coverslips after corresponding treatment for 24 h were washed with fresh medium and loaded with the oxidative stress detection reagent (green fluorescence) and superoxide detection reagent (red fluorescence) for 30 min at 37°C. Representative micrographs of ROS (a) and superoxide (b) in normal control neurons and neurons after OGD toxicity treated with vehicle, ROS inhibitor, MSCs, MNPs, or MNPs-MSCs. Fluorescence intensity quantification of ROS (c) and superoxide (d) using ImageJ software. Compared with the OGD-vehicle group, treatment with MNPs-MSCs, MSCs, or MNPs significantly decreased OGD-induced ROS and superoxide production in neurons. Moreover, treatment with MNPs-MSCs remarkably reduced ROS and superoxide production, which was superior to the effect of MSCs or MNPs. Treatment with MNPs-MSCs decreased superoxide generation in OGD-damaged neurons, which was comparable to the effect of ROS inhibitors. Scale bar = 50 μ m. The data are presented as the mean \pm SEM from six separate experiments. [#] $p < .01$ compared with the normal control; ^{**} $p < .01$ compared with the OGD-vehicle group or OGD-MNPs-MSCs group; ^{*} $p < .05$ compared with the OGD-MNPs-MSCs group; ⁿ $p > .05$ compared with the OGD-MNPs-MSCs group. MNP, melanin nanoparticle; MSC, mesenchymal stem cell; OGD, oxygen-glucose deprivation; ROS, reactive oxygen species

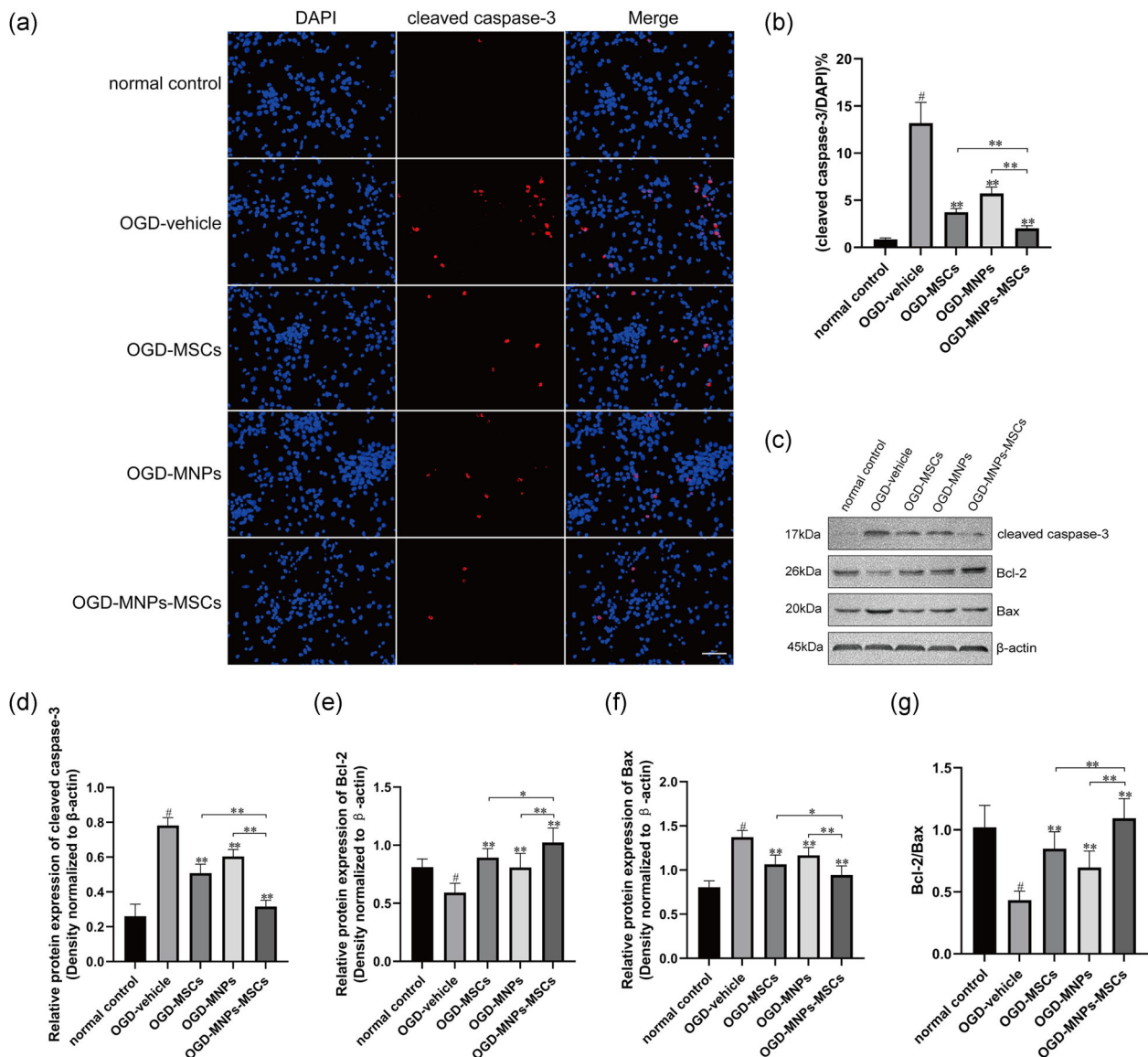


FIGURE 6 Treatment with MNPs-MSCs provides better protection against OGD-induced neuronal apoptosis than treatment with MNPs or MSCs only. Primary cortical neurons were cultured on cover slides at a density of 1×10^6 cells per well in a 12-well culture plate or a density of 2×10^6 cells per well in a six-well culture plate for 7 days. The treatment methods for each group were as described above. (a) Representative images of cleaved caspase-3 immunostaining in our experimental settings. Scale bar = 50 μ m. (b) Treatment with MNPs-MSCs, MSCs, or MNPs significantly decreased the number of cleaved caspase-3-positive cells compared with OGD vehicle, and the cleaved caspase-3 expression in the OGD-MNPs-MSCs group was significantly lower than that in the OGD-MSCs group or OGD-MNPs group. (c-f) The protein levels of cleaved caspase-3, Bcl-2, and Bax were detected by western blot analysis and quantified using ImageJ software. Western blot analysis showed that the levels of cleaved caspase-3 protein were significantly decreased with treatment with MNPs-MSCs, MSCs, or MNPs relative to the OGD vehicle group, and the levels of cleaved caspase-3 protein in the OGD-MNPs-MSCs group were significantly lower than those in the OGD-MSCs group or OGD-MNPs group. Treatment with MNPs-MSCs or MSCs prevented Bax upregulation and Bcl-2 downregulation relative to the OGD vehicle. (g) The ratio of Bcl-2/Bax. The Bcl-2/Bax ratio in the OGD-MNPs-MSCs group was significantly higher than that in the OGD-MSCs group or OGD-MNPs group. The data are presented as the mean \pm SEM from six separate experiments. [#] $p < .01$ relative to the normal control; ^{**} $p < .01$ compared with the OGD-vehicle group or OGD-MNPs-MSCs group, ^{*} $p < .05$ compared with the OGD-MNPs-MSCs group. MNP, melanin nanoparticle; MSC, mesenchymal stem cell; OGD, oxygen-glucose deprivation

Liu et al., 2017). Although the synthesized MNPs exhibit a relatively small size and narrow size distribution compared to squid eumelanin, which ranges from 100 to 300 nm, the chemical functions of synthesized melanin and squid eumelanin (Figure 1b-f) are identical and characterized by various spectral methods (Ju et al., 2011). In line with

previous reports (S. J. Liu et al., 2018; Ozlu et al., 2019), the current study demonstrated that MNPs exerted no cytotoxic effects on MSCs below a concentration of 100 μ g/ml, and there were no negative changes in cellular ultrastructure after MNPs were internalized into MSCs.

It has been well documented that OS, including ROS and reactive nitrogen species, followed by reperfusion is responsible for most ischemia–reperfusion injuries and thus leads to brain tissue damage (Orellana-Urzuu et al., 2020). The brain is highly sensitive to ROS-induced injury because the brain exhibits a high concentration of lipid peroxide, a low level of protective antioxidants, high oxygen consumption, and a high level of iron, which makes OS have a profound effect on the pathogenesis of stroke (Saeed et al., 2007). Therefore, modulating OS by scavenging ROS might be an effective measure to attenuate hypoxic-ischemic and reperfusion injury. According to previous reports (Rageh & El-Gebaly, 2018; Zhong et al., 2019), our data showed that MNPs exhibited the capacity to scavenge ROS and superoxide, which is beneficial for protecting against hypoxic-ischemic injury. Previous studies have shown that antioxidation is one of the protective mechanisms of MSCs against ischemic brain injury (Calió et al., 2014). We, therefore, wondered whether combined treatment with MSCs and MNPs exhibits a synergistic protective effect against hypoxic-ischemic injury. To our surprise, our study demonstrated that combined treatment with MSCs and MNPs provided better neuroprotection against ischemia than treatment with either MSCs or MNPs alone, and the underlying mechanism was related to their synergistic effect on antioxidants. These data provide favorable evidence for the clinical use of combined treatment with MSCs and MNPs as a therapy for ischemic stroke.

Previous studies have revealed that apoptosis may contribute to a significant proportion of neuronal death, especially in the ischemic penumbra, following acute brain ischemia (Uzdensky, 2019). Therefore, the identification of an efficient neuroprotector capable of rescuing neurons in the ischemic penumbra is the main goal for stroke therapy. Inhibitors of caspases, which play an important role in both the signal conduction and execution stage of the cascade reaction of apoptosis, can block the process of cell death in animal models of ischemic stroke, reduce the volume of cerebral infarction and significantly improve neurological function deficits after ischemic stroke (Shabanzadeh et al., 2015). Previous literature has shown that the expression of proapoptotic genes in the Bcl family, including Bax and Bcl-XS, was significantly increased, while the expression of antiapoptotic genes, including Bcl-2 and Bcl-XL, was significantly decreased after global cerebral ischemia in rats (Gillardon et al., 1996). A recent study revealed that the neuroprotection of MNPs was correlated with the prevention of Bax upregulation and Bcl-2 downregulation in Neuro2A cells treated with CoCl_2 (Liu et al., 2017). In line with a previous report (Liu et al., 2017), the current study demonstrated that MNPs inhibited caspase-3 cleavage, reduced the expression of Bax, and upregulated the expression of Bcl-2, which might therefore inhibit apoptosis after ischemia. Moreover, previous investigations have demonstrated that MSC transplantation can upregulate the expression of the antiapoptotic gene Bcl-2 in spontaneous stroke model rats, thereby inhibiting neuronal apoptosis (Calió et al., 2014). Our study indicated that combined treatment with MSCs and MNPs significantly inhibited the cleavage of Caspase-3, attenuated the expression of Bax, and upregulated the expression of Bcl-2 in OGD-injured neurons, and the protection against apoptosis

was superior to that of MSCs or MNPs. This result provides novel evidence that combined treatment with MSCs and MNPs might be a potential treatment for ischemic stroke.

5 | CONCLUSION

Our data suggested that combined treatment with MSCs and MNPs provides better protection for neurons against ischemic injury. Our study also demonstrated that MNPs enhanced the neuroprotection of MSCs against ischemic injury by suppressing neuronal apoptosis and antioxidant defense. Our data provide evidence that combined treatment with MSCs and MNPs might be a potential treatment for ischemic stroke. However, the interaction between MNPs and MSCs in vivo, such as the potential influence of MNPs on the survival, migration, and differentiation of MSCs in the host after combined treatment with MSCs and MNPs, remains unclear. Therefore, further work is needed to elucidate the underlying mechanisms of the synergistic effect.

ACKNOWLEDGMENTS

The authors would like to thank all the anonymous reviewers for their valuable comments on how to improve the quality of this paper. This study was supported by the National Natural Science Foundation of China (Grant Number: 81801361) and the Young Scientist Fund of the Natural Science Foundation of Guangxi (Grant Number: 2018GXNSFBA281045).

DATA AVAILABILITY STATEMENT

The data that support the findings of this study are available from the corresponding author upon reasonable request.

ORCID

Chunliu Tang  <http://orcid.org/0000-0003-3596-0303>

Deyan Kong  <http://orcid.org/0000-0003-1115-3259>

REFERENCES

- Bao, X., Wei, J., Feng, M., Lu, S., Li, G., Dou, W., Ma, W., Ma, S., An, Y., Qin, C., Zhao, R. C., & Wang, R. (2011). Transplantation of human bone marrow-derived mesenchymal stem cells promotes behavioral recovery and endogenous neurogenesis after cerebral ischemia in rats. *Brain Research*, 1367, 103–113. <https://doi.org/10.1016/j.brainres.2010.10.063>
- Brand-Williams, W. M., Cuvelier, M. E., & Berset, C. (1995). Use of free radical method to evaluate antioxidant activity. *LWT- Food Science and Technology*, 28(1), 25–30.
- Cai, W., Sun, J., Sun, Y., Zhao, X., Guo, C., Dong, J., Peng, X., & Zhang, R. (2020). NIR-II FL/PA dual-modal imaging long-term tracking of human umbilical cord-derived mesenchymal stem cells labeled with melanin nanoparticles and visible HUMSC-based liver regeneration for acute liver failure. *Biomaterials Science*, 8(23), 6592–6602. <https://doi.org/10.1039/d0bm01221a>
- Calió, M. L., Marinho, D. S., Ko, G. M., Ribeiro, R. R., Carbonel, A. F., Oyama, L. M., Ormanji, M., Guirao, T. P., Calió, P. L., Reis, L. A., Simões Mde, J., Lisbôa-Nascimento, T., Ferreira, A. T., & Bertoncini, C. R. (2014). Transplantation of bone marrow

- mesenchymal stem cells decreases oxidative stress, apoptosis, and hippocampal damage in brain of a spontaneous stroke model. *Free Radical Biology and Medicine*, 70, 141–154. <https://doi.org/10.1016/j.freeradbiomed.2014.01.024>
- Fu, J., Chen, Z., Wang, M., Liu, S., Zhang, J., Zhang, J., Han, R., & Xu, Q. (2015). Adsorption of methylene blue by a high-efficiency adsorbent (polydopamine microspheres): Kinetics, isotherm, thermodynamics and mechanism analysis. *Chemical Engineering Journal*, 259, 53–61. <https://doi.org/10.1016/j.cej.2014.07.101>
- Fu, J., Xin, Q., Wu, X., Chen, Z., Yan, Y., Liu, S., Wang, M., & Xu, Q. (2016). Selective adsorption and separation of organic dyes from aqueous solution on polydopamine microspheres. *Journal of Colloid and Interface Science*, 461, 292–304. <https://doi.org/10.1016/j.jcis.2015.09.017>
- Gillardone, F., Lenz, C., Waschke, K. F., Krajewski, S., Reed, J. C., Zimmermann, M., & Kuschinsky, W. (1996). Altered expression of Bcl-2, Bcl-X, Bax, and c-Fos colocalizes with DNA fragmentation and ischemic cell damage following middle cerebral artery occlusion in rats. *Brain Research. Molecular Brain Research*, 40(2), 254–260. [https://doi.org/10.1016/0169-328x\(96\)00059-9](https://doi.org/10.1016/0169-328x(96)00059-9)
- Goyal, M., Demchuk, A. M., Menon, B. K., Eesa, M., Rempel, J. L., Thornton, J., Roy, D., Jovin, T. G., Willinsky, R. A., Sapkota, B. L., Dowlatshahi, D., Frei, D. F., Kamal, N. R., Montanera, W. J., Poppe, A. Y., Ryckborst, K. J., Silver, F. L., Shuaib, A., Tampieri, D., ... ESCAPE Trial, I. (2015). Randomized assessment of rapid endovascular treatment of ischemic stroke. *New England Journal of Medicine*, 372(11), 1019–1030. <https://doi.org/10.1056/NEJMoa1414905>
- Ju, K. Y., Lee, Y., Lee, S., Park, S. B., & Lee, J. K. (2011). Bioinspired polymerization of dopamine to generate melanin-like nanoparticles having an excellent free-radical-scavenging property. *Biomacromolecules*, 12(3), 625–632. <https://doi.org/10.1021/bm101281b>
- Kong, D., Zhu, J., Liu, Q., Jiang, Y., Xu, L., Luo, N., Zhao, Z., Zhai, Q., Zhang, H., Zhu, M., & Liu, X. (2017). Mesenchymal stem cells protect neurons against hypoxic-ischemic injury via inhibiting parthanatos, necroptosis, and apoptosis, but not autophagy. *Cellular and Molecular Neurobiology*, 37(2), 303–313. <https://doi.org/10.1007/s10571-016-0370-3>
- Lee, J. Y., Kim, E., Choi, S. M., Kim, D. W., Kim, K. P., Lee, I., & Kim, H. S. (2016). Microvesicles from brain-extract-treated mesenchymal stem cells improve neurological functions in a rat model of ischemic stroke. *Scientific Reports*, 6, 33038. <https://doi.org/10.1038/srep33038>
- Li, R., Parvez, K., Hinkel, F., Feng, X., & Mullen, K. (2013). Bioinspired wafer-scale production of highly stretchable carbon films for transparent conductive electrodes. *Angewandte Chemie*, 52(21), 5535–5538. <https://doi.org/10.1002/anie.201300312>
- Liu, N., Zhang, Y., Fan, L., Yuan, M., Du, H., Cheng, R., Liu, D., & Lin, F. (2011). Effects of transplantation with bone marrow-derived mesenchymal stem cells modified by survivin on experimental stroke in rats. *Journal of Translational Medicine*, 9(1), 105.
- Liu, S. J., Wang, L. J., Qiao, Y., Zhang, H., Li, L. P., Sun, J. H., He, S., Xu, W., Yang, X., Cai, W. W., Li, J. D., Wang, B. Q., & Zhang, R. P. (2018). A promising magnetic resonance stem cell tracer based on natural biomaterials in a biological system: Manganese(II) chelated to melanin nanoparticles. *International Journal of Nanomedicine*, 13, 1749–1759. <https://doi.org/10.2147/IJN.S157508>
- Liu, Y., Ai, K., Ji, X., Askhatova, D., Du, R., Lu, L., & Shi, J. (2017). Comprehensive insights into the multi-antioxidative mechanisms of melanin nanoparticles and their application to protect brain from injury in ischemic stroke. *Journal of the American Chemical Society*, 139(2), 856–862. <https://doi.org/10.1021/jacs.6b11013>
- Liu, Y., Ai, K., Liu, J., Deng, M., He, Y., & Lu, L. (2013). Dopamine-melanin colloidal nanospheres: An efficient near-infrared photothermal therapeutic agent for in vivo cancer therapy. *Advanced Materials*, 25(9), 1353–1359. <https://doi.org/10.1002/adma.201204683>
- Lou, X. F., Wang, C., Zhang, J. C., Du, Y. Z., & Xu, X. L. (2021). A melanin-like nanoenzyme for acute lung injury therapy via suppressing oxidative and endoplasmic reticulum stress response. *Pharmaceutics*, 13(11):1850. <https://doi.org/10.3390/pharmaceutics13111850>
- Moniche, F., Gonzalez, A., Gonzalez-Marcos, J. R., Carmona, M., Piñero, P., Espigado, I., Garcia-Solis, D., Cayuela, A., Montaner, J., Boada, C., Rosell, A., Jimenez, M. D., Mayol, A., & Gil-Peralta, A. (2012). Intracranial bone marrow mononuclear cells in ischemic stroke: A pilot arterial trial. *Stroke*, 43(8), 2242–2244. <https://doi.org/10.1161/STROKEAHA.112.659409>
- Muchada, M., Rubiera, M., Rodriguez-Luna, D., Pagola, J., Flores, A., Kallas, J., Sanjuan, E., Meler, P., Alvarez-Sabin, J., Ribo, M., & Molina, C. A. (2014). Baseline National Institutes of Health stroke scale-adjusted time window for intravenous tissue-type plasminogen activator in acute ischemic stroke. *Stroke*, 45(4), 1059–1063. <https://doi.org/10.1161/STROKEAHA.113.004307>
- Orellana-Urzuá, S., Rojas, I., Libano, L., & Rodrigo, R. (2020). Pathophysiology of ischemic stroke: Role of oxidative stress. *Current Pharmaceutical Design*, 26(34), 4246–4260. <https://doi.org/10.2174/1381612826666200708133912>
- Ozlu, B., Kabay, G., Bocek, I., Yilmaz, M., Piskin, A. K., Shim, B. S., & Mutlu, M. (2019). Controlled release of doxorubicin from polyethylene glycol functionalized melanin nanoparticles for breast cancer therapy: Part I. Production and drug release performance of the melanin nanoparticles. *International Journal of Pharmaceutics*, 570, 118613. <https://doi.org/10.1016/j.ijpharm.2019.118613>
- Prasad, K., Mohanty, S., Bhatia, R., Srivastava, M. V., Garg, A., Srivastava, A., & Mishra, N. K. (2012). Autologous intravenous bone marrow mononuclear cell therapy for patients with subacute ischaemic stroke: A pilot study. *The Indian Journal of Medical Research*, 136(2), 221–228.
- Rageh, M. M., & El-Gebaly, R. H. (2018). Melanin nanoparticles: Antioxidant activities and effects on gamma-ray-induced DNA damage in the mouse. *Mutation Research, Genetic Toxicology and Environmental Mutagenesis*, 828, 15–22. <https://doi.org/10.1016/j.mrgentox.2018.01.009>
- Saeed, S. A., Shad, K. F., Saleem, T., Javed, F., & Khan, M. U. (2007). Some new prospects in the understanding of the molecular basis of the pathogenesis of stroke. *Experimental Brain Research*, 182(1), 1–10. <https://doi.org/10.1007/s00221-007-1050-9>
- Savitz, S. I., Misra, V., Kasam, M., Juneja, H., Cox, C. S. Jr., Alderman, S., Aisiku, I., Kar, S., Gee, A., & Grotta, J. C. (2011). Intravenous autologous bone marrow mononuclear cells for ischemic stroke. *Annals of Neurology*, 70(1), 59–69. <https://doi.org/10.1002/ana.22458>
- Shabanzadeh, A. P., D'Onofrio, P. M., Monnier, P. P., & Koeberle, P. D. (2015). Targeting caspase-6 and caspase-8 to promote neuronal survival following ischemic stroke. *Cell Death & Disease*, 6, e1967. <https://doi.org/10.1038/cddis.2015.272>
- Sun, T., Jiang, D., Rosenkrans, Z. T., Ehlerding, E. B., Ni, D., Qi, C., Kuttyreff, C. J., Barnhart, T. E., Engle, J. W., Huang, P., & Cai, W. (2019). A melanin-based natural antioxidant defense nanosystem for theranostic application in acute kidney injury. *Advanced Functional Materials*, 29(48):1904833. <https://doi.org/10.1002/adfm.201904833>
- Tarangini, K., & Mishra, S. (2014). Production of melanin by soil microbial isolate on fruit waste extract: Two step optimization of key parameters. *Biotechnol Reports*, 4, 139–146. <https://doi.org/10.1016/j.btre.2014.10.001>
- Uzdensky, A. B. (2019). Apoptosis regulation in the penumbra after ischemic stroke: Expression of pro- and antiapoptotic proteins. *Apoptosis*, 24(9–10), 687–702. <https://doi.org/10.1007/s10495-019-01556-6>
- Zhao, H., Zeng, Z., Liu, L., Chen, J., Zhou, H., Huang, L., Huang, J., Xu, H., Xu, Y., Chen, Z., Wu, Y., Guo, W., Wang, J. H., Wang, J., & Liu, Z.

- (2018). Polydopamine nanoparticles for the treatment of acute inflammation-induced injury. *Nanoscale*, 10(15), 6981–6991. <https://doi.org/10.1039/c8nr00838h>
- Zhong, G., Yang, X., Jiang, X., Kumar, A., Long, H., Xie, J., Zheng, L., & Zhao, J. (2019). Dopamine-melanin nanoparticles scavenge reactive oxygen and nitrogen species and activate autophagy for osteoarthritis therapy. *Nanoscale*, 11(24), 11605–11616. <https://doi.org/10.1039/c9nr03060c>
- Zhu, W., Chen, J., Cong, X., Hu, S., & Chen, X. (2006). Hypoxia and serum deprivation-induced apoptosis in mesenchymal stem cells. *Stem Cells*, 24, 1141.

How to cite this article: Tang, C., Luo, J., Yan, X., Huang, Q., Huang, Z., Luo, Q., Lan, Y., Chen, D., Zhang, B., Chen, M., & Kong, D. (2022). Melanin nanoparticles enhance the neuroprotection of mesenchymal stem cells against hypoxic-ischemic injury by inhibiting apoptosis and upregulating antioxidant defense. *Cell Biology International*, 46, 933–946. <https://doi.org/10.1002/cbin.11781>